Title
An Uncertainty Estimator for Slitting Method Residual Stress Measurements Including the Influence of Regularization

Permalink
https://escholarship.org/uc/item/73b3c2v8

Journal
Experimental Mechanics, 60(1)

ISSN
0014-4851

Authors
Olson, MD
DeWald, AT
Hill, MR

Publication Date
2020

DOI
10.1007/s11340-019-00535-x

Peer reviewed

An uncertainty estimator for slitting method residual stress measurements including the influence of regularization

M.D. Olson[1], A.T. DeWald[1], and M.R. Hill[2]

[1]*Hill Engineering, LLC, 3083 Gold Canal Drive, Rancho Cordova, CA*
[2]*Department of Mechanical and Aerospace Engineering, University of California,
One Shields Avenue, Davis, CA*

ABSTRACT

This paper describes the development of a new uncertainty estimator for slitting method residual stress measurements. The new uncertainty estimator accounts for uncertainty in the regularization-based smoothing included in the residual stress calculation procedure, which is called regularization uncertainty. The work describes a means to quantify regularization uncertainty and then, in the context of a numerical experiment, compares estimated uncertainty to known errors. The paper further compares a first-order uncertainty estimate, established by a repeatability experiment, to the new uncertainty estimator and finds good correlation between the two estimates of precision. Furthermore, the work establishes a procedure for automated determination of the regularization parameter value that minimizes total uncertainty. In summary, the work shows that uncertainty in the regularization parameter is a significant contributor to the total uncertainty in slitting method measurements and that the new uncertainty estimator provides a reasonable estimate of single measurement uncertainty.

Keywords: Residual stress measurement, uncertainty, slitting method, crack compliance method, integral method, regularization, repeatability, precision

NOMENCLATURE

L	Specimen length (normal to slit direction)
W	Specimen width (parallel to slit direction)
B	Specimen out of plane thickness
E	Young's Modulus
E'	plane strain Young's Modulus
ν	Poisson's ratio
$\boldsymbol{\sigma}$	Vector of unknown residual stresses assumed to act over each slit depth increment,
$\boldsymbol{\varepsilon}$	Vector of the measured strain at each cut depth
$\boldsymbol{G}$	Compliance matrix (contains the strains that would be caused from assumed residual stress basis functions)
$\boldsymbol{G}_{pl\text{-}\varepsilon}$	Plane-strain unit pulse compliance matrix
$\boldsymbol{F}$	Matrix to alleviate singularity is stress calculation when slit depths are large
$\boldsymbol{C}$	Matrix that evaluates the chosen derivative of the residual stress solution that is to be penalized
$\boldsymbol{S}$	Matrix that contains the standard errors associated with the deformation data at each cut depth
$\boldsymbol{H}$	Matrix that contains the normalized cut depth increment length
Γ	Scale correction to account for out-of-plane thickness of specimen
β	Regularization parameter
α	Modified regularization parameter ($\beta = 10^{\alpha}/E'^{2}$)
$\hat{\boldsymbol{\varepsilon}}$	Fit strain
$\boldsymbol{\varepsilon}_{\mathrm{misfit}}$	Strain misfit (difference between measured strain and fitted strain)
e	Lower limit of strain uncertainty taken as the precision inherent to the experimental apparatus
$\boldsymbol{U}_{\varepsilon}$	Vector of strain uncertainties
$\boldsymbol{U}_{\sigma,\mathrm{reg}}$	Vector of stress uncertainty due to regularization uncertainty
$\boldsymbol{U}_{\sigma,\varepsilon}$	Vector of stress uncertainty due to strain uncertainty
$\boldsymbol{U}_{\sigma,\mathrm{tot}}$	Vector of total stress uncertainty

1. INTRODUCTION

Slitting [1], hole-drilling [2], and ring-coring [3] are all established residual stress measurement techniques that determine a residual stress versus depth profile using measurements of deformation (typically strain at a given location) caused by cutting-induced release of residual stress. Measured deformation versus depth data are used to calculate a residual stress versus depth profile, most commonly using the *integral method* [4,5,6,7], which uses a numerical inverse. In a typical residual stress calculation, a regularization parameter is used to control smoothing of the deformation data that is useful in mitigating the amplification of measurement uncertainty in the computed residual stress versus

depth profile. Because the appropriate value of the regularization parameter is unknown to the experimenter, and the value assigned significantly affects the residual stress computed, there is a need to quantify the uncertainty associated with the regularization parameter.

The objective of this work is to develop an improved residual stress uncertainty estimator for the slitting method by incorporating uncertainty associated with the regularization parameter. Typical uncertainty estimates for slitting are inadequate because they ignore this type of error, as noted recently by Prime [8]. This work consists of a description of the proposed error estimator and then two phases of application. In the first phase, a numerical experiment (with a known residual stress state) is performed to determine the relationship between measurement error and the selection of the regularization parameter. The numerical experiment guides the development of the regularization uncertainty estimate and provides some context to judge its usefulness. In the second phase, the proposed slitting method uncertainty estimator (including the regularization uncertainty) is evaluated using experimental data from a repeatability experiment.

2. METHODS

Slitting method overview

A useful summary of the theoretical background for the stress calculations performed in a slitting method residual stress measurement is given in [7]. The key details are summarized here to provide context. To fix ideas, consider a slitting experiment in a rectangular plate of length L, width W, and out of plane thickness B, as shown in Fig. 1. The residual stress to be evaluated is a profile of the residual stress component acting along the length of the plate as a function of width, $\sigma_{xx}(y)$. The slitting measurement consists of cutting a slit into the test specimen in small increments of depth at the specimen mid-length, $x = L/2$, in Fig. 1. At each increment of cut depth h_i, the initial residual stresses redistribute and cause deformation that is recorded after each cut depth increment, often using a strain

gage located at the back face of the slitting measurement plane (e.g., centered at $(x, y) = (L/2, W)$). The strain versus slit depth data are used to calculate residual stress.

The constitutive equation relating measured strain to residual stress is

$$GF\sigma = F\varepsilon \tag{1}$$

where G is a *compliance matrix* that contains the strains that would be caused from assumed residual stress basis functions, σ is a vector of unknown residual stresses assumed to act over each slit depth increment, F is a diagonal matrix of factors that alleviates a singularity that occurs when the slit depth approaches the part width, and ε is a vector of the measured strain at each cut depth. G and F are square matrices of size NxN, with N equal to the number of cut depth increments used in the experiment. Each entry in the compliance matrix, G_{ij}, is the strain that arises at the strain gage location when a uniform unit stress (stress basis function) acts over a slit depth increment specified by i (i.e., $\sigma_{xx}(y) = 1$ over $h_{i-1} < y < h_i$, where $h_0 = 0$), for a specific depth of slit h_j. Because this compliance matrix uses basis functions that are pulses of constant unit stress over each cut depth increment, it is called a *unit pulse compliance matrix*. The diagonal entries in F are given by $F_{(i)(i)} = [(W - h_i)/W]^2$ [7]. The compliance matrix can be computed for plane strain (i.e., $B \gg W$) and then modified to account for a smaller degree of plane strain in a specific thickness using

$$G = \Gamma(B,W)G_{pl\text{-}\varepsilon} \tag{2}$$

$$\Gamma(B,W) = 1 + \left(\frac{v^2}{1 - v^2}\right)\left(\frac{1}{1 + (B/0.697W)^2}\right) \tag{3}$$

where $G_{pl\text{-}\varepsilon}$ is the unit pulse compliance matrix computed using a plane-strain constitutive equation, $\Gamma(B, W)$ is a correction suggested in [9], and v is Poisson's ratio of the plate. Computation of the unit pulse plain-strain compliance is typically performed using elastic finite element stress analysis following procedures described elsewhere (e.g., [1]).

The formulation of Eq. (1) inherently assumes there is no noise in the measured strain, which is not possible in practice. To smooth out noise in the measured strain data, and prevent its amplification in computed residual stress, Schajer and Prime [7] suggested adding Tikhonov regularization to Eq. (1), resulting in

$$[(GF)^\mathrm{T}GF + \beta C^\mathrm{T}S^\mathrm{T}HSC]\sigma = (GF)^\mathrm{T}F\varepsilon \tag{4}$$

where C is a matrix that evaluates the chosen derivative of the residual stress solution that is to be penalized. Typically, C uses second derivative regularization where the first and last rows are zero and the other rows ($i = 2, N - 1$) have a tridiagonal structure given by Eq. (5):

$$\frac{-2(W/N)^2}{(h_{i+1} - h_{i-1})(h_i - h_{i-1})}, \frac{2(W/N)^2}{(h_i - h_{i-1})(h_{i+1} - h_i)}, \frac{-2(W/N)^2}{(h_{i+1} - h_i)(h_{i+1} - h_{i-1})}. \tag{5}$$

S is a diagonal matrix that contains the standard errors associated with the deformation data at each cut depth and is given by $S_{(i)(i)} = F_{(i)(i)}U_{\varepsilon(i)}$, where U_ε is a vector of strain uncertainty versus depth described below. H is a diagonal matrix that contains the normalized cut depth increment length (i.e., $H_{(i)(i)} = (h_i - h_{i-1})/W$, where $h_0 = 0$), and β is a scalar value called the regularization parameter. Often in practice, values of β can be very small ($\sim 10^{-15}$) and can vary significantly between materials with different elastic moduli. To alleviate these issues, in this work β is defined in terms of a new regularization parameter α, via

$$\beta = 10^\alpha/E^2. \tag{6}$$

where E is Young's modulus. The term E^2 is included to make Eq. (4) dimensionally consistent.

The above provides a means for computing the residual stress versus depth vector σ given a vector of strain versus depth data, ε and a specific value of α

$$\sigma = V\varepsilon \tag{7}$$

where

$$V = [(GF)^T GF + (10^\alpha/E^2)C^T S^T HSC]^{-1}(GF)^T F. \tag{8}$$

Given the stress versus depth vector σ, from Eq. (7), a fitted strain $\hat{\varepsilon}$ is determined from

$$\hat{\varepsilon} = G\sigma. \tag{9}$$

The fitted and measured strains are nearly equal, $\hat{\varepsilon} \approx \varepsilon$, when the value of α is highly negative but for a typical value of α there is a finite strain misfit defined as

$$\varepsilon_{\text{misfit}} = \varepsilon - \hat{\varepsilon}. \tag{10}$$

The value of the regularization parameter α, and subsequently β in Eq. (4), significantly influences the calculated residual stress. In an extreme case with no regularization ($\alpha \ll 0$, so $\beta \approx 0$), the measured strains are fit exactly and strain measurement noise is amplified in the calculated residual stress. In the other extreme case, with $\alpha \approx 0$, the measured strains will be overly smoothed and the calculated residual stress versus depth profile will likely miss important features. A specific value of α must be selected during data reduction, and since the best value is not known *a priori* the selection increases uncertainty in the measured residual stress.

Slitting method uncertainty estimation

The uncertainty in the calculated residual stress due to the uncertainty in the measured strain data has previously been established by Prime and Hill [10] for both Legendre polynomials as well as unit pulse basis functions. The uncertainty in stress caused by strain uncertainty is given by

$$U_{\sigma,\varepsilon}^2 = diag(V[DIAG(U_\varepsilon^2)]V^T) \tag{11}$$

where $U_{\sigma,\varepsilon}$ is a vector of residual stress uncertainty versus depth due to uncertainty in the measured strain at each cut depth, *diag* is an operator that provides a vector of the diagonal elements of a square

matrix, DIAG is an operator that provides a diagonal matrix from a vector, $\boldsymbol{V}$ is defined in Eq. (8), and $\boldsymbol{U}_\varepsilon$ is a vector of strain uncertainties

$$\boldsymbol{U}_\varepsilon = max(\boldsymbol{\varepsilon}_{\mathrm{misfit}}, e) \tag{12}$$

where e is a lower limit of strain uncertainty taken as the precision inherent to the experimental apparatus and typically on the order of 1 µε.

Improved slitting method uncertainty estimation

This work proposes an improved slitting method uncertainty estimator that adds an additional term to account for uncertainty associated with the selection of the regularization parameter, called the *regularization uncertainty*. With the addition of regularization uncertainty, the total uncertainty is taken as the root of the sum of squares (RSS) of the two uncertainty sources

$$\boldsymbol{U}_{\sigma,\mathrm{tot}}^2 = \boldsymbol{U}_{\sigma,\varepsilon}^2 + \boldsymbol{U}_{\sigma,\mathrm{reg}}^2. \tag{13}$$

For a specific value of $\alpha = \hat{\alpha}$, the regularization uncertainty is established by assessing a set of residual stress versus depth results computed using different values of α near $\hat{\alpha}$ (i.e., different amounts of regularization), which defines the sensitivity of the computed residual stress to α. Each member of the set of residual stress results is computed for a range of α called α_{subset}. The range α_{subset} is defined by two key characteristics, the number of values that it contains, M, and the range of α that it spans. The present work uses a logarithmically spaced set of $M = 60$ values of α spanning a range $\alpha_{\mathrm{subset}} = [\hat{\alpha} \pm R]$ where $R = 1.5$. The justification for these values of parameters M and R is presented later. A vector of regularization uncertainty versus depth, $\boldsymbol{U}_{\sigma,\mathrm{reg}}$, is then defined as the standard deviation of the set of residual stress values at each depth computed for the different values of α in α_{subset}

$$U_{\sigma,\text{reg}}(\hat{\alpha}) = \sqrt{\frac{1}{M-1}\sum_{i=1}^{M}[\boldsymbol{\sigma}_i - \bar{\boldsymbol{\sigma}}]^2} \qquad (14)$$

where the vectors $\boldsymbol{\sigma}_i$ reflect the stresses computed for the range α_{subset} and $\bar{\boldsymbol{\sigma}}$ is the average residual stress versus depth vector computed for the range α_{subset} (the bracketed terms on the right side of Eq. (14) are vectors, and the square and square root operations are performed element-by-element).

Automated regularization parameter selection

Although there have been suggestions on choosing an appropriate value of regularization parameter [7], a new method is suggested here to select a value of $\alpha = \hat{\alpha}$ during the data reduction process. The selected value $\hat{\alpha}$ is one that minimizes the root-mean-square (RMS) of the total uncertainty vector of Eq. (13). A comparison of different approaches to selecting $\hat{\alpha}$ is presented later, in the discussion section. To limit the possible α values to useful values, residual stress is calculated from Eq. (4) with values of α ranging from a highly negative value ($\alpha = -15$) to progressively less negative values, ending when the maximum strain misfit exceeds 100 $\mu\varepsilon$ (the high misfit indicating excessive regularization).

Slitting numerical experiment

To determine whether the regularization uncertainty as defined above was a useful predictor of regularization error, a numerical experiment was performed. The numerical experiment consisted of three steps. In the first step, a residual stress distribution (initialized residual stress) was chosen and introduced as an initial condition in an elastic finite element stress analysis of the plate shown in Fig. 1, and then strain versus slit depth data were extracted from the model. This defined the numerical experiment strain. The initialized residual stress was a parabolic shape similar to the residual stress profile that might be achieved from quenching [11], defined using a second order Legendre polynomial

$$\sigma_{xx}(y) = 100[3(2y/W-1)^2 - 1]/2 \text{ MPa.} \qquad (15)$$

8

The stress analysis used commercial software [12] and had the geometry shown in Fig. 1 with $L = 3W$ and a strain gage of size $g_L = 0.01W$. The simulated slit was at $x = L/2$ and had a slit width of $0.001W$. Elements were removed from the mesh to simulate cut depths from $h_1 = 0.02W$ to $h_{49} = 0.98W$ in cut depth increments of $0.02W$. The model used a refined, biased mesh where the node spacing was $0.0033W$ at the cut plane and increased to $0.01W$ at $x = 0$ and $x = L$ with a total number of elements of 115,600. Details of finite element models typical of slitting are given by Lee and Hill [13]. Each element was a two-dimensional, plane strain quadrilateral with biquadratic displacement interpolation. The elastic material properties were $E = 70{,}000$ GPa, and $v = 0.3$. The computed initial residual stress (at zero slit depth) is shown in Fig. 2a, and strain as a function of slit depth is shown in Fig. 2b.

The second step of the numerical experiment determined the compliance matrix in Eq. (4). The compliance matrix used the same approach and model as was used for the first step, but with constant stress (unit pulses) applied over each cut depth increment and for each cut depth (instead of the initialized residual stress distribution at each cut depth).

In the third step of the numerical experiment, noise was added to the numerical experiment strain and residual stress and uncertainties were calculated for a range of α values. The added noise was normally distributed with a magnitude of 1 µε (Fig. 3). The strain precision was set to $e = 0.5$ µε. Since the numerical experiment used a known residual stress, the error arising from the added noise could be directly determined and provides a useful benchmark to assess the proposed uncertainty estimator.

Slitting repeatability experiment

To further evaluate the usefulness of the proposed uncertainty estimator, the calculated uncertainty was compared to the precision defined by a repeatability experiment comprising a set of repeated slitting

measurements on samples prepared identically. The repeatability experiment consisted of 10 slitting measurements on aluminum blocks removed from a larger quenched aluminum plate. The parent aluminum plate was composed of alloy 7050‑T7451 and had a width, length, and height of 190.5 mm (7.5 in), 381 mm (15 in), and 22.9 mm (0.9 in). The plate was heat treated, including a quench, to induce residual stresses. The heat treatment consisted of heating the plate to 477°C (890°F) for 3 hours, quenching in room temperature water, artificial aging at 121°C (250°F) for 8 hours followed by additional aging at 177°C (350°F) for 8 hours (following the approach in [14]). A set of blocks for use in the repeatability experiment was extracted near the center of the parent plate, each block having a length, width, and out of plane thickness of $L = 63.5$ mm (2.5 in), $W = 22.9$ mm (0.9 in), and $B = 45.7$ mm (1.8 in), as shown in Fig. 4. Each slitting measurement was performed on a separate block. The measurements determined the length direction residual stress (σ_{xx} in Fig. 4) as a function of depth into 22.9 mm block width (y in Fig. 4) at the mid-length of the sample ($x = 31.75$ mm (1.25 in)).

   The slitting method experiments followed the approach described by Hill [1] and Prime [15]. Each measurement used a single strain gage mounted on the back face of the sample ($y = 22.9$ mm) with a 0.787 mm (0.031 in) gage length, and self-temperature compensated for aluminum. Each slitting measurement consisted of 30 cut depth increments, ranging in size from 0.05 to 1.27 mm. A compliance matrix for each experiment was determined from a 2D, plane strain, finite element model and unit pulse basis functions. The model had E of 71,710 MPa (10,400 ksi) and ν of 0.33, to match the specimen material properties. The compliance matrix model had approximately 300,000 eight-node, biquadratic elements, with 1,000 elements across the width and biased node spacing away from the cut plane, with square elements at the cut plane and element size approximately 10x larger at the free ends. Lastly, since the compliance matrix is computed using a plane strain model, it was scaled using the correction scheme developed by Aydiner and Prime [9] to account for the finite out of plane thickness of the block, as given above in Eq. (3).

Uncertainty estimator acceptance criterion

To test the usefulness of the uncertainty estimator an acceptance criterion was used. The acceptance criterion determined the *acceptance fraction* which is the percentage of points where the calculated residual stress ± uncertainty contains the true value. The true value was known for the numerical experiment. However, the true value is unknown in the repeatability study and was assumed to be the mean of the data at each depth from all 10 measurements. This was chosen as the reference value because it is expected to be the best representation of the underlying residual stress field. Further, the standard deviation of the 10 measurements provides an approximation of the measurement precision (i.e., first order uncertainty estimate), assuming each specimen has an identical initial residual stress state. Assuming the uncertainty estimator is useful and that the underlying uncertainty has a normal distribution, we would expect 68% of the points in the depth profile to meet the acceptance criterion (i.e., acceptance fraction = 68% to correspond with ± one standard deviation).

3. RESULTS

Numerical experiment

The calculated residual stress from the numerical experiment with various levels of regularization and the associated misfits can be seen in Fig. 5. The calculated residual stresses (Fig. 5a) show that very low regularization ($\alpha = -15$) results in residual stress with large fluctuations that arise from the added noise. Use of more positive values of α are effective in mitigating the effect of the added noise and provide better approximation of the initialized residual stress. However, more positive α increases the misfit in strain (Fig. 5b), and when high regularization is chosen the large misfit indicates the calculated residual stress profile is overly smoothed. The strain misfit for the chosen value of α closely resembles the added noise.

The estimated measurement uncertainties from the numerical experiment with various levels of regularization are shown in Fig. 6. The regularization uncertainty $U_{\sigma,\text{reg}}$ (Fig. 6a) is low (nearly zero) for a low α value, moderate for the chosen α value (peak uncertainties around 2 MPa), and large for a high α value (peak uncertainties around 6 MPa). The low $U_{\sigma,\text{reg}}$ for low α occurs because the calculated residual stress is relatively insensitive to values of α within α_{subset}. The uncertainty in stress due to strain uncertainty $U_{\sigma,\varepsilon}$ (Fig. 6b) is high for a low α value (peak uncertainties around 19 MPa). This occurs because the calculated residual stress is sensitive to noise without regularization (i.e., V in Eq. (8) is poorly conditioned). For the chosen or high values of α, $U_{\sigma,\varepsilon}$ is low (peak uncertainties around 1 MPa). The total uncertainty in residual stress $U_{\sigma,\text{tot}}$ (Fig. 6c) follows $U_{\sigma,\varepsilon}$ for low α values, and $U_{\sigma,\text{reg}}$ for the chosen and high α values.

The maximum and RMS values of $U_{\sigma,\varepsilon}$, $U_{\sigma,\text{reg}}$ and $U_{\sigma,\text{tot}}$ are shown as functions of α for the numerical experiment in Fig. 7a. The maximum and RMS values of uncertainty each follow similar trends. $U_{\sigma,\text{reg}}$ is low for highly negative α, increasing to a maximum, decreasing to a local minimum, and then increasing again. $U_{\sigma,\varepsilon}$ is constant for highly negative α values, decreasing to a local minimum, and then increasing again. $U_{\sigma,\text{tot}}$ follows the uncertainty due to strain uncertainty, $U_{\sigma,\varepsilon}$, for highly negative α values and follows the regularization uncertainty for the most positive α values.

The maximum and RMS error in stress for the numerical experiment is shown in Fig. 7b (solid lines), where error at each depth is the calculated residual stress minus the initialized residual stress. The error is large and constant for highly negative α, decreases with increasing α to a minimum and then increases. Fig. 7b shows that $U_{\sigma,\text{tot}}$ follows the trend of the error and is larger than the error near the minimum uncertainty. Furthermore, the minimums of uncertainty and error occur at similar α values. This shows $U_{\sigma,\text{tot}}$ is a useful predictor of error.

The calculated residual stress at the chosen α value is shown in Fig. 8a for the numerical experiment. The calculated residual stress matches the initialized residual stress well. The total uncertainty provides a good approximation of the error overall, as shown in Fig. 8b, with both having a maximum value at the initial cut depth (1.7 MPa error and 2.0 MPa total uncertainty) and uncertainty and error falling between 1.5 and 0.25 MPa at larger cut depths. Regularization and strain uncertainties are both significant contributors to the total uncertainty.

The calculated residual stress ± the total uncertainty in Fig. 8 contains the initialized residual stress at 81.6% of points. Over 50 additional assessments with independent, noisy data added to the initialized strain, the calculated residual stress ± the total uncertainty includes the initialized stress at 73.0% of points. This is nominally consistent with the level of agreement that would be expected if the uncertainty followed a normal distribution (68% of points within ± one standard deviation).

Repeatability study

The results of the repeatability study can be seen in Fig. 9. The results show that all ten measurements (Fig. 9a) are consistently measuring a nearly parabolic residual stress distribution with a minimum value near the surface of ⁻70 MPa and maximum value near the mid-width of 25 MPa. The repeatability standard deviation (Fig. 9b) has a maximum value at the surface (3.2 MPa) and is between 0.3 to 1.8 MPa for larger cut depths, where the repeatability standard deviation is the standard deviation of measurements of nominally identical test specimens performed by the same operator, at the same laboratory over a short interval of time. The estimated total uncertainty for each of the ten measurements is also shown in Fig. 9b. The estimated total uncertainty and repeatability standard deviation follow similar trends, with the uncertainty being somewhat larger at initial cut depths (3.0 to 5.2 MPa versus 3.2 MPa) and somewhat (about 1 MPa) smaller between y = 8 to 15 mm.

The acceptance criterion was assessed for each measurement as the fraction of points in the residual stress depth profile where the calculated residual stress ± the total uncertainty contains the mean residual stress and is shown in Fig. 10. The acceptance criterion was met on average at 61.3% of points, with individual measurements meeting the criterion at 30 to 100% of the points.

The RMS regularization, strain, and total uncertainties for each of the ten measurements as a function of α are shown in Fig. 11. The RMS regularization, strain, and total uncertainty generally follow the same trends found in the numerical experiment; however, the regularization uncertainty has a broad range of α, between about -10 and -6, where the uncertainty is nearly constant (for most measurements). Despite this difference, the RMS total uncertainty has a well-defined minimum (Fig. 11b) that provides for a clear selection of α. The RMS repeatability standard deviation (labeled as Std in Fig. 11c) shows the repeatability standard deviation is similar to the total uncertainty for α near where the total uncertainty minimized for each measurement.

The RMS misfit values are shown for the repeatability experiment in Fig. 12a. The results show that for the α selection strategy used here (selected α values are shown as square markers), the RMS misfits are small (ranging from 0.8 to 1.2 με). The misfit as a function of cut depth for each of the 10 measurements is shown in Fig. 12b. The misfits exhibit significant form that does not appear to be random noise (peak misfits near ±2 με). This indicates the calculated residual stress could be somewhat over smoothed; however, the misfit trend also has a saw-tooth profile that is consistent with a quantizing error [16].

4. DISCUSSION

Both the numerical experiment and the repeatability experiment provide useful information to inform a strategy for selection of an appropriate value of regularization parameter. The numerical experiment is especially useful since the noise in the data and error in residual stress are known. A

pragmatic way to define an optimal amount of regularization is to determine the value of α where the

RMS misfit matches the RMS added noise. For the numerical experiment, the RMS values of error,

uncertainties, and misfit are plotted as functions of α in Fig. 13; also indicated are the RMS of added

noise and the optimal α (where the RMS misfit is equal to the RMS noise). The optimal α occurs at

$\alpha \approx -6$. It is noteworthy that this working definition of an optimal α does not provide for a minimum

error in residual stress; this occurs at $\alpha \approx -6.7$. Furthermore, Fig. 13 shows that the RMS total

uncertainty and RMS regulation uncertainty are minimized near the value of α where the RMS error is a

minimum.

In preliminary parts of this work, the RMS misfit as a function of α, and its first and second

derivatives (with respect to α) were studied as potential ways to select α. These parameters are shown

for the numerical experiment in Fig. 14. The misfit increases rapidly with α for $\alpha < -12$, increases

moderately with α for $-12 < \alpha < -6$, and increases rapidly with α for $-6 < \alpha$. The minimum of the first

derivative of the misfit RMS (circle marker in Fig. 14) shows where misfit is changing most slowly.

Selecting this value of α would result in insufficient smoothing of the data (α too negative) relative to

the optimal value of α. The maximum of the second derivative of the RMS misfit gives the maximum

rate of change of the misfit slope (triangle marker in Fig. 14). This value of α is near the optimal α (Fig.

14b) and would be a good selection. Use of the misfit derivatives was promising in the context of the

numerical experiment; however, use of the misfit derivatives was rendered ineffective when assessing

data from the repeatability experiment (that contain typical noise), and was subsequently abandoned

(e.g., the first and second derivatives of the RMS misfit for the repeatability experiment are shown in

Fig. 15 and show no useful trend that could be reliably assessed).

To better illustrate some possible α selection strategies, the numerical experiment was repeated with

50 sets of independent noise added to the numerical experiment strain and the 50 data sets were assessed

15

using seven different α selection strategies. Fig. 16a shows the optimal α (where RMS misfit equals RMS noise) versus the selected α for each of the 50 data sets and Fig. 16b shows the average and standard deviation of the difference between the selected and the optimal α for each α selection strategy. The solid line in Fig. 16a and Fig. 16b is where the optimal α equals the selected α and above that line the data would be over-smoothed (α too positive) and below that line the data would be under-smoothed (α too negative). The results show that selecting α at the minimum RMS total uncertainty or the minimum RMS regularization uncertainty each under-smooths the data. Selecting α at the minimum RMS strain uncertainty over-smooths the data. Selecting α at the minimum of the RMS misfit first derivative under-smooths the data with a large dispersion. Selecting α at maximum of the RMS misfit second derivative essentially fits the data optimally with a narrow dispersion. But using RMS misfit derivatives when assessing the repeatability experiments showed those approaches to be flawed. Two additional α selection strategies were tested. One strategy chose α when the RMS misfit was equal to the precision of the measurement, which was 1 με in the numerical experiment (the magnitude of the added noise). This α selection strategy performed well, with the α values being near optimal, but with significant dispersion; furthermore, this strategy is impractical because the strain precision is seldom known for a given experiment. A final α selection strategy is as described in [7], based on a "standard error" computed from the strain data. This approach appears to over-smooth the data and is very consistent. These assessments led to the approach described above: select α that minimizes the RMS total uncertainty.

Computing the total uncertainty requires establishing the sensitivity of residual stress to the selected value of α. In the present formulation, we define this sensitivity by computing the standard deviation of values of residual stress determined for values of α in $\alpha_{\text{subset}} = [\hat{\alpha} \pm R]$. Two important characteristics of α_{subset} are the number of terms it contains, M, and the size of the sampled range, R. To minimize computation time, it is useful to minimize M. To determine a useful value of M, trial calculations were

16

run using different values of M from 2 to 100. Fig. 17 shows that the RMS regularization uncertainty changes significantly with M, but a plateau occurs near $M = 40$. We selected $M = 60$ because the RMS regularization uncertainty was within 1% of the value at 100 terms (Fig. 17).

To determine the appropriate range of α values to sample when calculating the regularization uncertainty (i.e., to define R), the numerical experiment was repeated with various values of R from 0 to 3 (for $R = 0$, the regularization uncertainty is zero). For each value of R, the numerical experiment was repeated with 50 sets of independent random noise added to the strain data (same set of strain data for each R). The fraction of points meeting the acceptance criterion was determined for each of the 50 numerical experiments and the mean of the 50 acceptance fractions is shown in Fig. 18a. This assessment shows that an R value of 1.0 provides the expected acceptance fraction of 68%. A similar assessment was performed using data from the repeatability experiment, where R was varied and the fraction of points meeting the acceptance criterion was determined for each of the 10 measurements. The mean of the 10 acceptance fractions is shown in Fig. 18b as a function of R ("Quenched Al" in the figure) and shows that an R value of 1.6 provides the expected acceptance fraction of 68%. Furthermore, similar assessments were performed to elucidate a useful value of R. An additional numerical experiment used a residual stress profile with a sharp near-surface gradient where the stresses decays from -70 MPa to 20 MPa over 20% of the thickness (details are omitted for brevity), and R of 1.31 provided the expected acceptance fraction ("LSP" in Fig. 18a). Data from two other repeatability experiments were assessed, one using shot peened aluminum blocks (unpublished) and the other using laser shock peened (LSP) stainless steel blocks [17]. The results of these assessments are shown in Fig. 18b and values of R providing the expected acceptance fraction of 68% were 1.52 for the shot peened aluminum and 2.35 for the LSP stainless steel. It is promising that similar values of R provide the expected acceptance fraction in both the repeatability studies and the numerical experiments. The somewhat smaller values of R in the numerical experiments is consistent with the reduced number of

extraneous factors in a numerical experiment compared with those in the physical repeatability experiments (e.g., one clear extraneous factor in the physical experiments is the variation in residual stress that should be expected in identically prepared samples). Based on these results $R = 1.5$ was used for computing regularization uncertainty. This value is conservative (i.e., over-estimates the measurement uncertainty) for the two numerical experiments and correlates well with results from 2 of the 3 repeatability studies.

The numerical experiment used random noise that had a magnitude of 1 με and a strain precision of $e = 0.5$ με. To evaluate the effect of these parameters, the relationship between R and the acceptance fraction was determined for different amounts of strain noise (0.25 με and 1 με) and as well as using different values of strain precision ($e = 0, 0.25, 0.5, 1,$ and 2 με). The results can be seen in Fig. 19a for 1 με added noise and in Fig. 19b for 0.25 με added noise. The results show that for a given R the acceptance fraction increases with e for a given level of strain noise. The results also show the R required to meet the expected acceptance fraction is similar when e is smaller than the added noise (i.e., in Fig. 19a the acceptance fraction is ≈ 68% for R near 1 when $e = 0, 0.25,$ or 0.5 με). When e is equal to the added noise the acceptance fraction at $R = 1.5$ is about 5% larger than the expected.

To further evaluate the acceptance fraction and the implementation of the total uncertainty estimator in the context of the numerical experiment, the total uncertainty was scaled by a factor corresponding to different confidence intervals, assuming that the uncertainty follows the normal distribution. The acceptance fraction versus R is shown for different confidence intervals is shown in Fig. 20. The scaling factors used for the normal distribution are: 0.674 (50% confidence interval), 1 (68% confidence interval), 1.282 (80% confidence interval), 1.645 (90% confidence interval), and 1.96 (95% confidence interval). The results show that R of 1.0 provides the expected acceptance fraction for the 50%, 68%, and 80% confidence intervals, with R of 1.2 and 1.4 providing expected acceptance fractions for the

90% and 95% confidence intervals. The consistent values of R for the range of confidence intervals supports the soundness of the new uncertainty estimator.

It is interesting that the RMS of the repeatability standard deviation (Std in Fig. 11c) monotonically decreases as α increases, even though the calculated residual stress becomes over smoothed as α nears zero (as indicated by the large RMS misfits in Fig. 12a). Highly smoothed results are precise (i.e., repeatable), but are not necessarily accurate. This affirms the principle that a good experimental method provides both good precision and good accuracy to the extent possible.

The correlation between the uncertainty estimate with the error in the numerical experiment and with the repeatability standard deviation of the repeatability experiment has led to the following procedure to determine the regularization parameter. First, select a highly negative $\hat{\alpha}$ value (e.g., $\hat{\alpha} = -15$), then begin computing stress over α_{subset}. The range of α_{subset} starts from $\hat{\alpha} - R = \hat{\alpha} - 1.5$, ends at $\hat{\alpha} + R = \hat{\alpha} + 1.5$ and has 60 equally spaced values. Next, determine the strain, regularization, and total uncertainty for $\hat{\alpha}$ (using the stresses computed over the range of α_{subset} values for the regularization uncertainty and at $\hat{\alpha}$ for the strain uncertainty). Then repeat the same procedure with incrementally more positive $\hat{\alpha}$ values (e.g., incrementally increase $\hat{\alpha}$ by 0.1), until a large RMS misfit occurs (e.g., 100 $\mu\varepsilon$). After the stress calculation is complete for the various $\hat{\alpha}$ values, compute the RMS uncertainties and select the stress where the minimum of the RMS total uncertainty occurs.

5. CONCLUSIONS

This work provides a new single-measurement uncertainty estimator for slitting method residual stress measurements. The total uncertainty is defined as the root sum square of uncertainties from strain measurement imprecision and regularization. Uncertainty due to strain measurement imprecision was defined in earlier work. The regularization uncertainty arises from uncertainty in the appropriate level of smoothing to be applied to measured strain versus cut depth data. We provide a means to estimate the

regularization uncertainty and recommend choosing a value of regularization parameter (α) that minimizes the RMS of total uncertainty (RMS of values of uncertainty over all depth positions).

The new single-measurement uncertainty estimator was demonstrated and tested in the context of a numerical experiment, which showed that the point values and spatial trends of estimated uncertainty follow the known errors. The estimated uncertainty also meets the defined acceptance criterion: the estimated stress ± uncertainty contains the known stress at 68% of points. Further, the numerical experiment showed that reporting only uncertainty due to measurement imprecision is non-conservative.

The new single-measurement uncertainty estimator was demonstrated and validated in the context of a physical repeatability experiment. The point values and spatial trends of the estimated uncertainty for each single measurement were consistent with the precision defined by the standard deviation of the repeated measurements.

The regularization uncertainty is a significant contributor to the total uncertainty in slitting residual stress measurements. Regularization uncertainty may also be important for similar residual stress measurement techniques (e.g., hole drilling).

REFERENCES

[1] M. R. Hill, "The Slitting Method," in Practical Residual Stress Measurement Methods, G. S. Schajer, Ed. West Sussex, UK: John Wiley & Sons, 2013, pp. 89–108.

[2] ASTM, "E837 − 08: Test Method for Determining Residual Stresses by the Hole-Drilling Strain-Gage Method," ASTM International, West Conshohocken, PA, Jul. 2009.

[3] G. S. Schajer and P. S. Whitehead, "Hole Drilling and Ring Coring," in Practical Residual Stress Measurement Methods, G. S. Schajer, Ed. John Wiley & Sons, Ltd, 2013, pp. 29–64.

[4] G. S. Schajer, "Measurement of Non-uniform Residual Stresses Using the Hole-Drilling Method. Part II - Practical Application of the Integral Method," J. Eng. Mater. Technol., vol. 110, pp. 344–349, 1988.

[5] M. Barsanti, M. Beghini, C. Santus, A. Benincasa, and L. Bertelli, "Integral Method Coefficients and Regularization Procedure for the Ring-Core Residual Stress Measurement Technique," in Advanced Materials Research, 2014, vol. 996, pp. 331–336.

[6] M. Beghini, L. Bertini, and L. F. Mori, "Evaluating Non-Uniform Residual Stress by the Hole-Drilling Method with Concentric and Eccentric Holes. Part I. Definition and Validation of the Influence Functions," Strain, vol. 46, no. 4, pp. 324–336, Aug. 2010.

[7] G. S. Schajer and M. B. Prime, "Use of Inverse Solutions for Residual Stress Measurements," J. Eng. Mater. Technol., vol. 128, no. 3, pp. 375–382, Jul. 2006.

[8] M. B. Prime, "The Inadequacy of Uncertainty Estimation in Residual Stress Measurements," presented at the Residual Stress Summit 2017, Dayton, OH, USA, 24-Oct-2017.

[9] C. Can Aydıner and M. B. Prime, "Three-Dimensional Constraint Effects on the Slitting Method for Measuring Residual Stress," *J. Eng. Mater. Technol.*, vol. 135, no. 3, p. 031006, Jul. 2013.

[10] M. B. Prime and M. R. Hill, "Uncertainty, Model Error, and Order Selection for Series-Expanded, Residual-Stress Inverse Solutions," J. Eng. Mater. Technol., vol. 128, no. 2, pp. 175–185, Apr. 2006.

[11] W. M. Sim, "Residual stress engineering in manufacture of aerospace structural parts," Filton, UK: Airbus SAS, 2009.

[12] Abaqus/Standard, "Version 6.10." Simulia Inc., Providence, RI, USA, 2010.

[13] M. J. Lee, M. R. Hill, Effect of Strain Gage Length When Determining Residual Stress by Slitting. J Eng Mater Technol. vol 129, pp. 143–150, 2007.

[14] SAE Aerospace, "Aerospace Material Specification 4342: Aluminum Alloy Extrusions: Solution Heat Treated, Stress Relieved, Straightened, and Overaged," 2006.

[15] M. B. Prime, "Experimental Procedure for Crack Compliance (Slitting) Measurements of Residual Stress," Los Alamos National Laboratory Report (LA-UR-03-8629), 2003.

[16] A. Gersho and R. M. Gray, "Scalar Quantization: Structure and Performance," in Chapter 5: Scalar Quantization: Structure and Performance, *Vector Quantization and Signal Compression*, Springer Science & Business Media, 2012, pp. 133–172.

[17] M. J. Lee and M. R. Hill, "Intralaboratory Repeatability of Residual Stress Determined by the Slitting Method," Exp. Mech., vol. 47, no. 6, pp. 745–752, Dec. 2007.

FIGURES
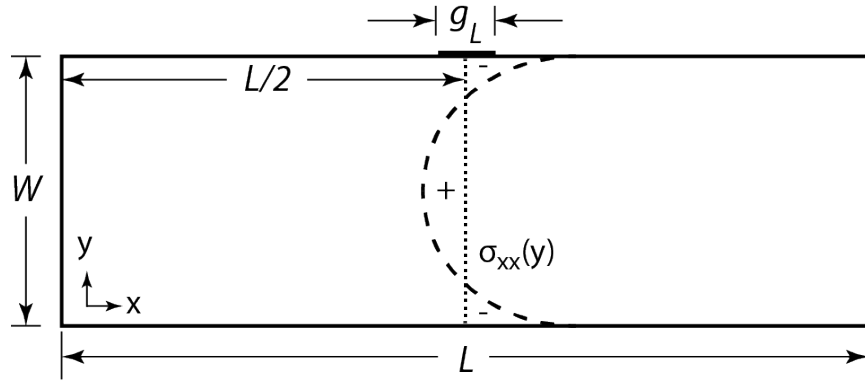
Fig. 1 – Diagram of a typical slitting measurement. The measurement plane is at x = L/2 and incrementally cuts the sample from y = 0 to W to measure σ$_{xx}$(L/2, y). The strain gage has a length of g$_L$ and its mid-length is affixed to the back face of the specimen at (x, y) = (L/2, W). B is the out of plane thickness

(a)

(b)
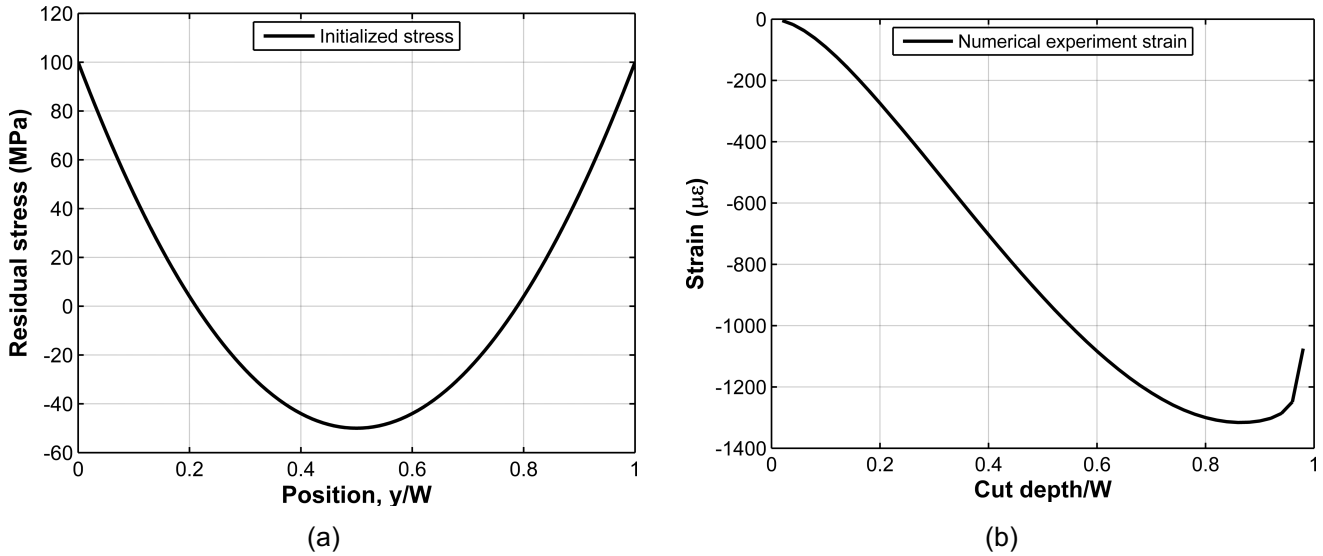
Fig. 2 – Data for the numerical experiment: (a) initialized residual stress and (b) numerical experiment strain
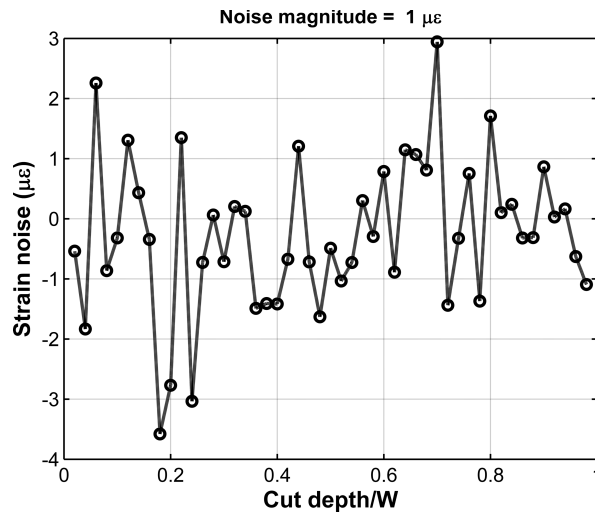
Fig. 3 – Data for the numerical experiment: noise added to the numerical experiment strain
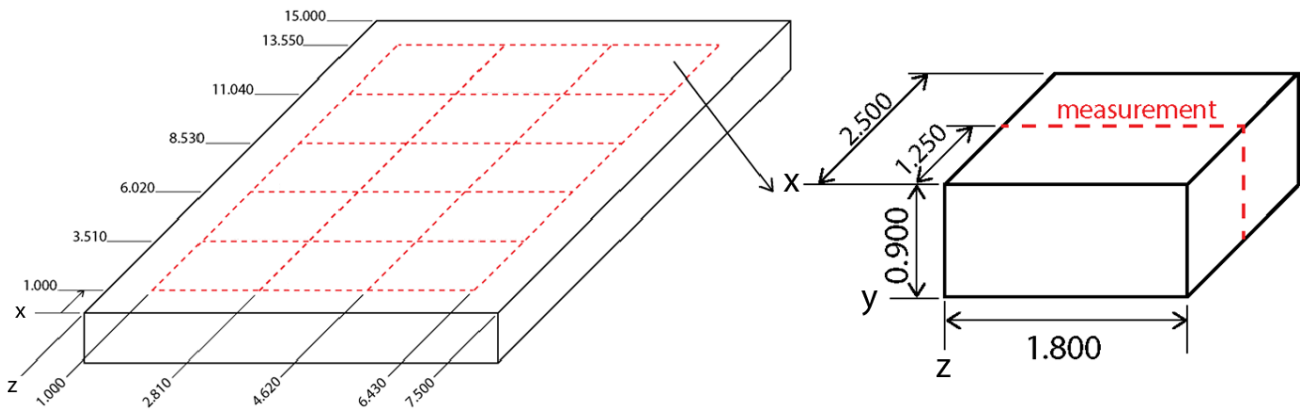
Fig. 4 – Geometry of the quenched aluminum blocks used in the repeatability experiment (dimensions in inches)
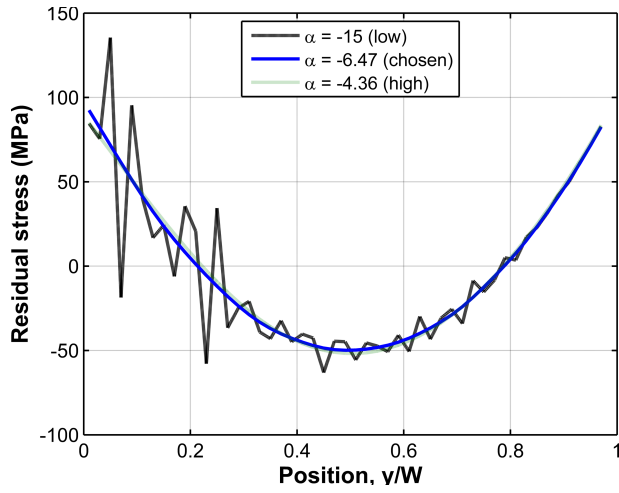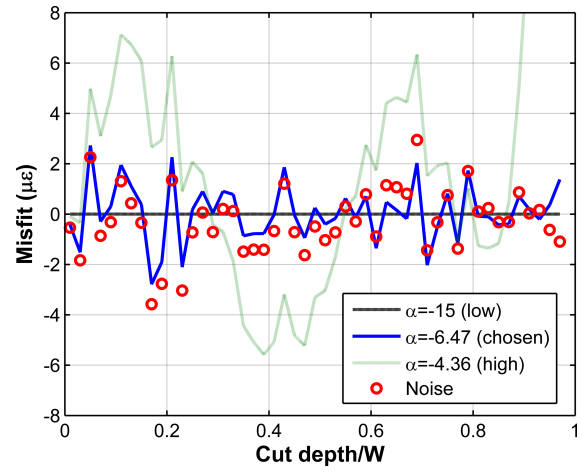
Fig. 5 – Results for the numerical experiment with various choices of α: (a) calculated residual stress and (b) resulting misfit and applied noise
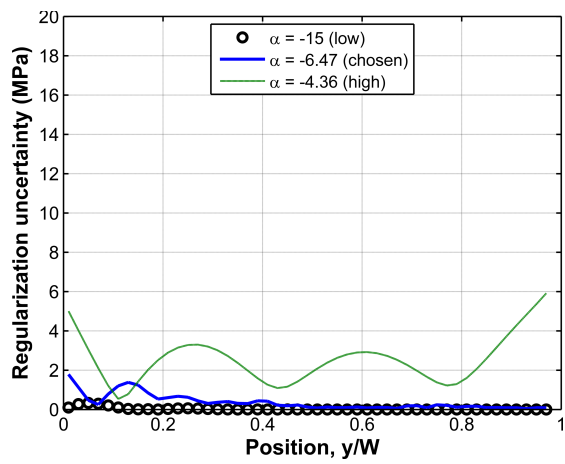
(a)
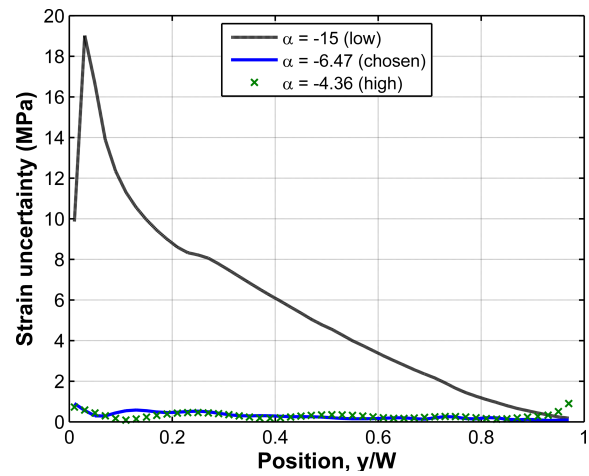
(b)
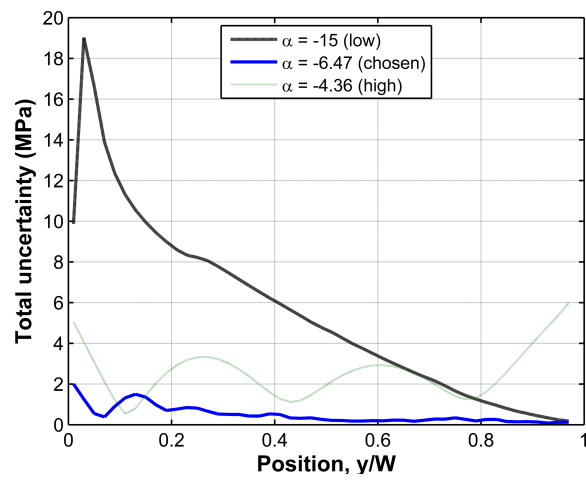
(c)

*Fig. 6 – Uncertainties in stress for the numerical experiment for a range of α values:
(a) regularization, (b) strain, and (c) total uncertainty*
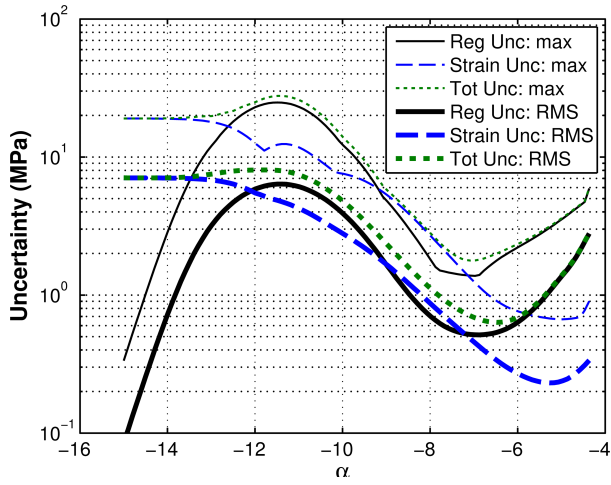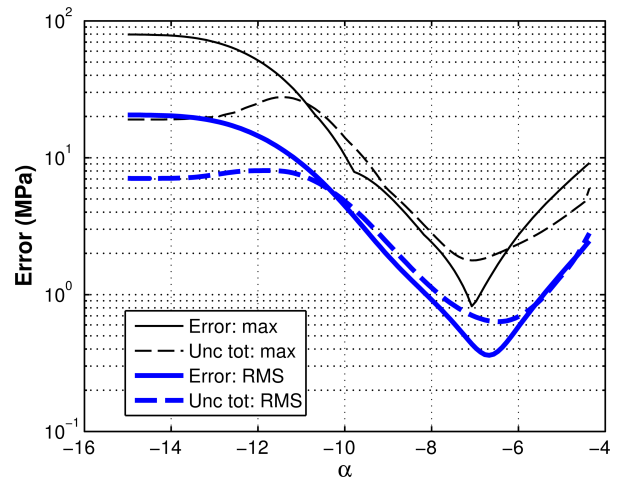
Fig. 7 – Results for the numerical experiment: (a) Maximum and RMS regularization, strain, and total uncertainty as a function of α and (b) maximum and RMS error and total uncertainty
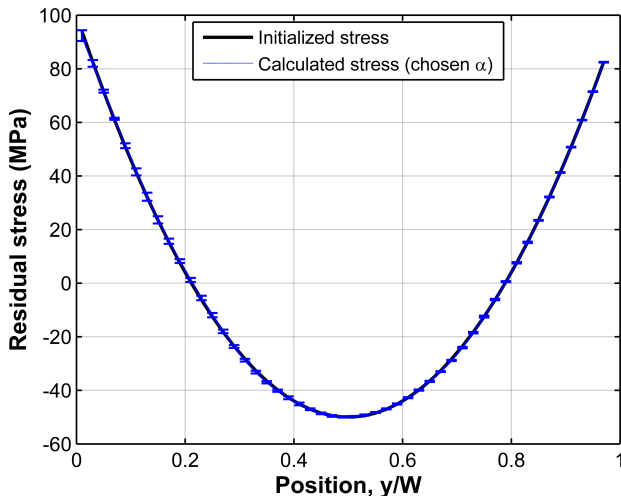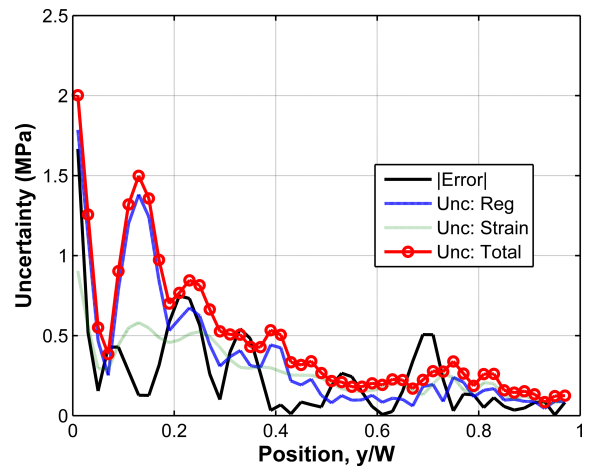
Fig. 8 – Results for the numerical experiment: (a) initialized and calculated residual stress, and (b) uncertainty and error
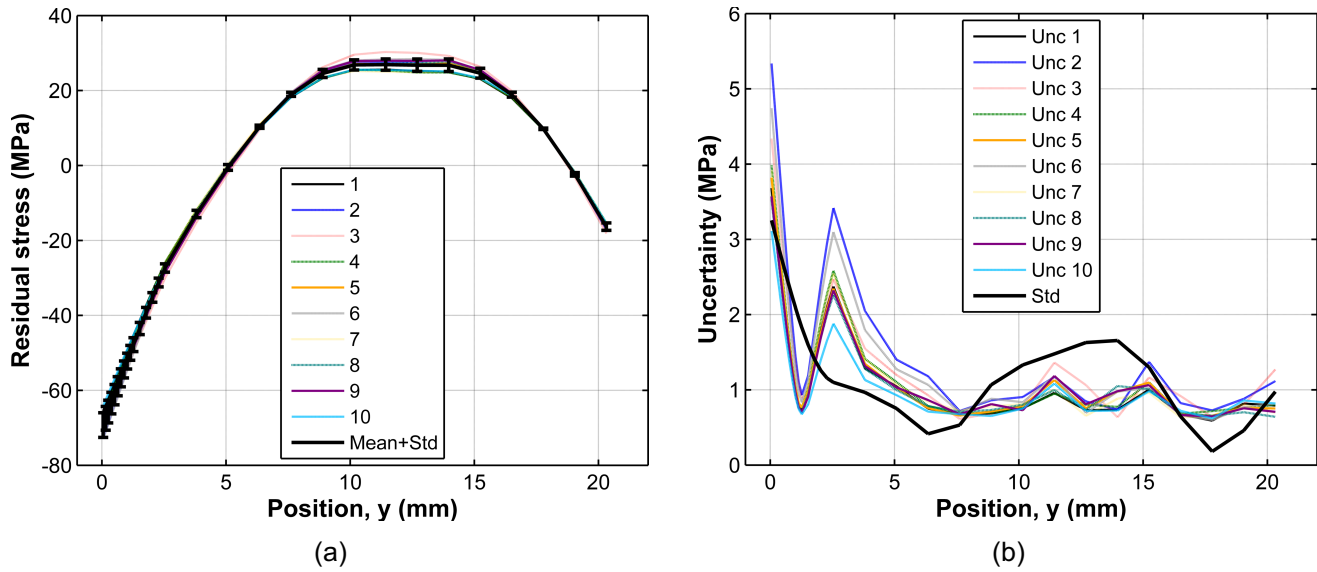
Fig. 9 – Results for the repeatability experiment: (a) calculated residual stress with mean and error bars showing the repeatability standard deviation, and (b) total uncertainty and repeatability standard deviation
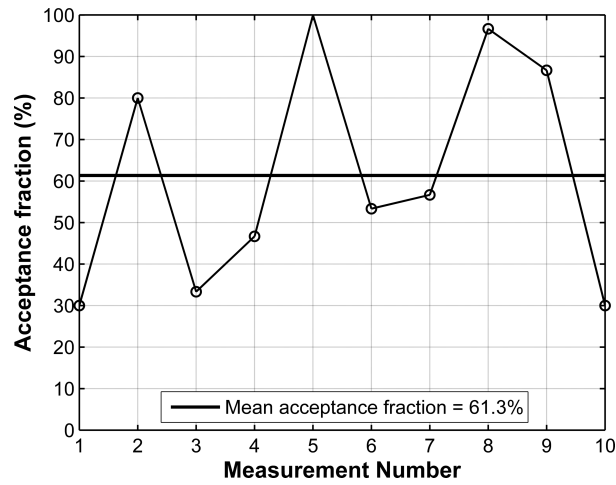
Fig. 10 – Acceptance fraction for the repeatability experiment: percentage of points where the acceptance criterion was met (i.e., calculated residual stress ± the total uncertainty contains the mean residual stress) for each measurement. The mean acceptance fraction is 61.3%
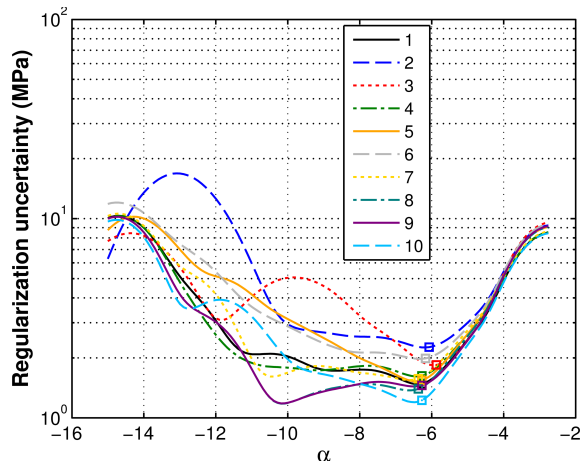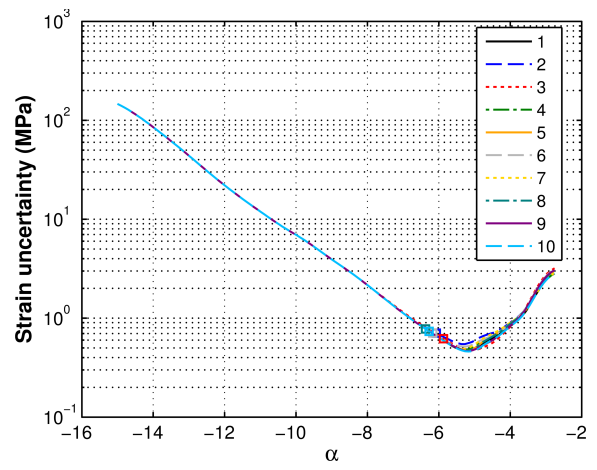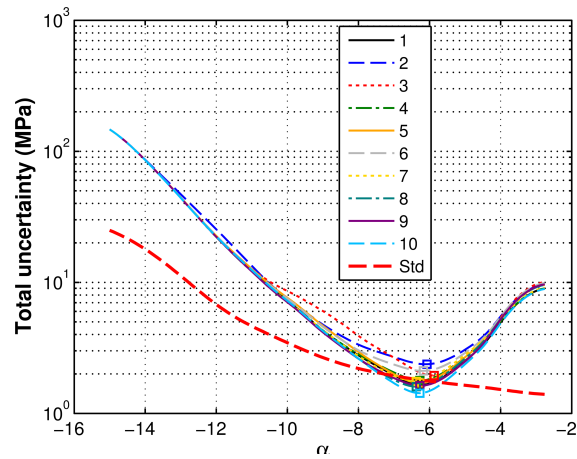
Fig. 11 – Results for the repeatability experiment as a function of α: RMS uncertainty in stress due to (a) regularization, (b) strain, and (c) total with repeatability standard deviation
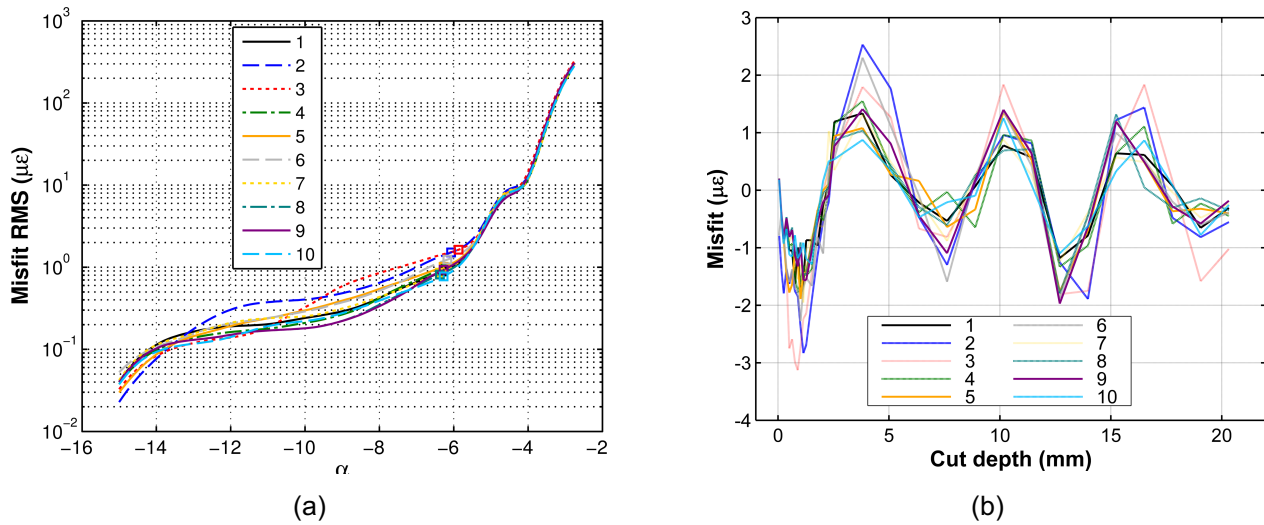
Fig. 12 – Results for the repeatability experiment for each of the ten measurements: (a) RMS misfit as a function of α and (b) misfit versus cut depth at the chosen α
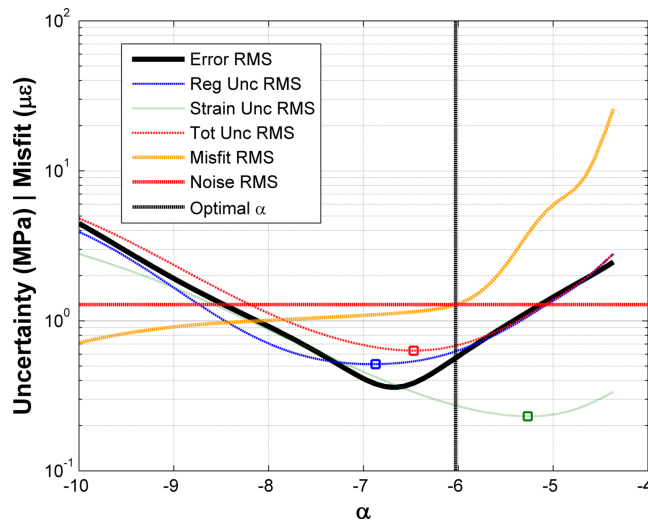
Fig. 13 – Results for the numerical experiment as a function of α: RMS error and uncertainties in stress
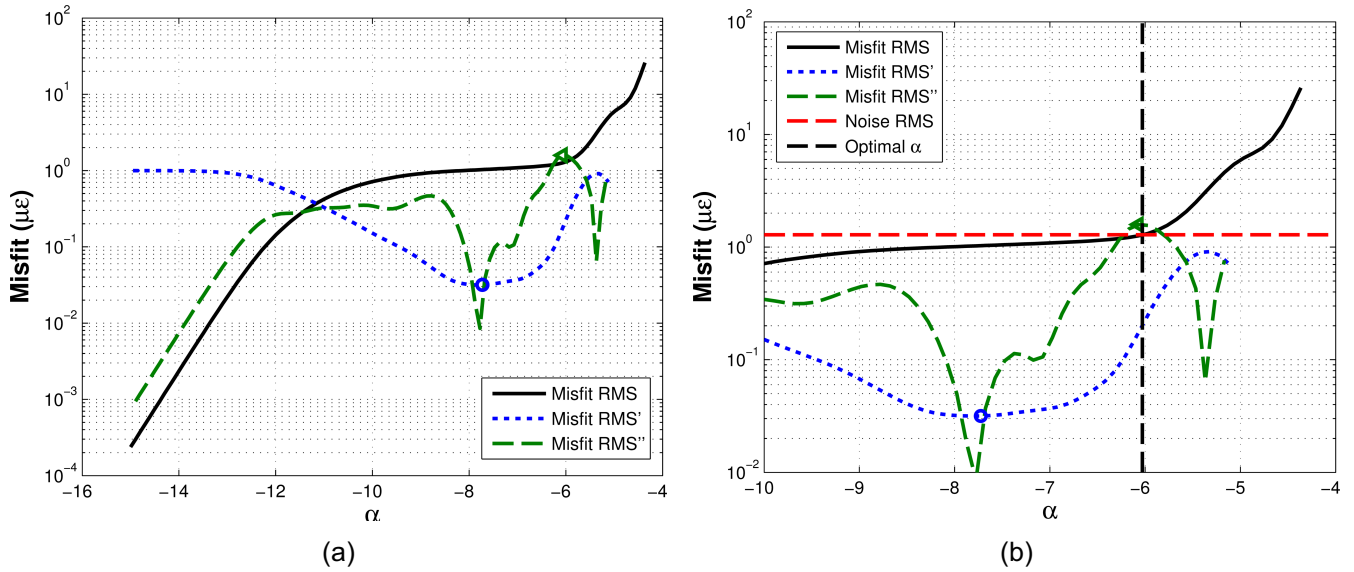
Fig. 14 – Results for the numerical experiment as a function of α: RMS misfit and its first (Misfit RMS') and second derivatives (Misfit RMS'') with respect to α over (a) full α range and (b) over a smaller α range (dashed lines showing the RMS noise and optimal α)
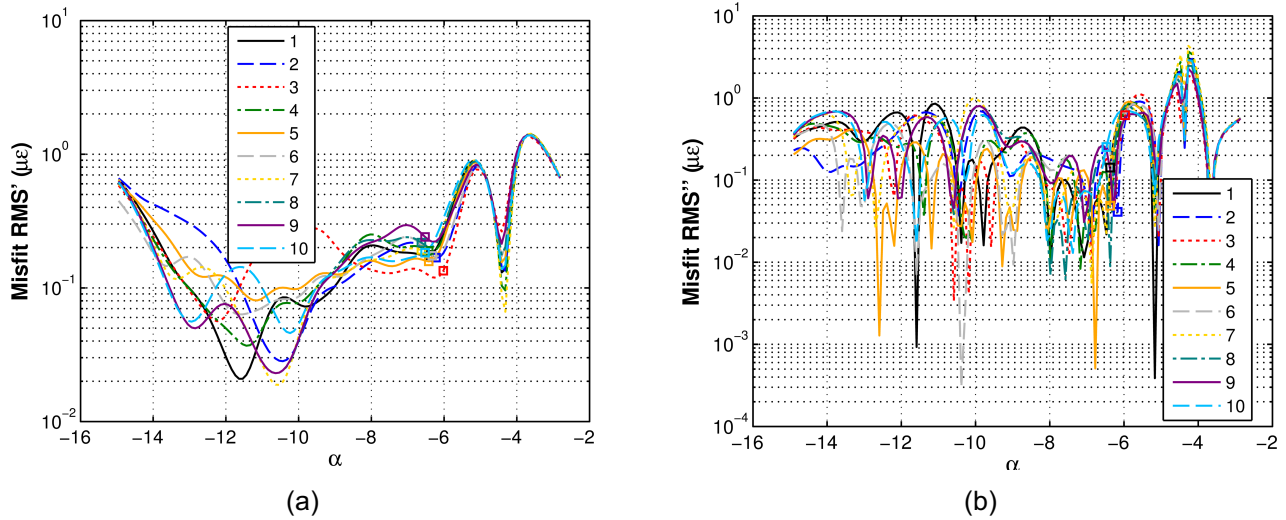
Fig. 15 – Results for the repeatability experiment as a function of α: derivatives of RMS misfit with respect to α: (a) first derivative and (b) second derivative
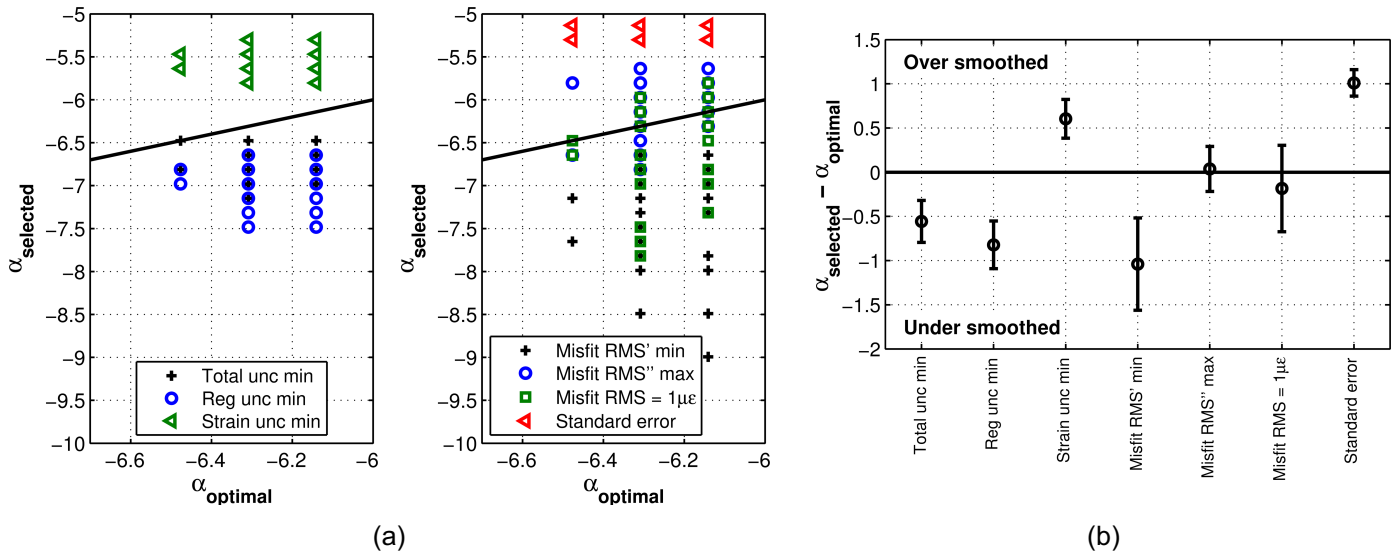
Fig. 16 – Results for additional numerical experiments and several α selection strategies: (a) α optimal versus α selected for several α selection strategies with 50 sets of randomly added noise, and (b) the average and standard deviation of the difference between the selected and optimal α values (note: the solid line in (a) and (b) is where the optimal and selected values of α are equal)
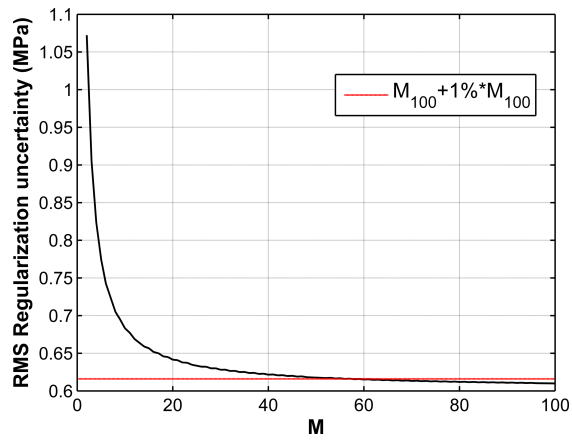
Fig. 17 – Additional calculation showing the RMS regularization uncertainty as a function of the number of terms in α_{subset} (M)
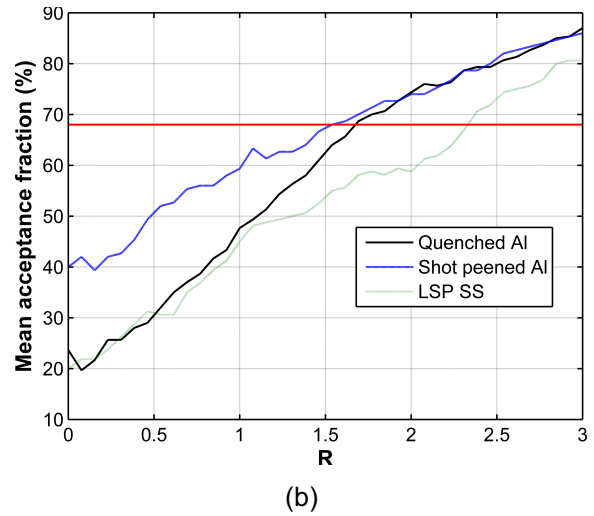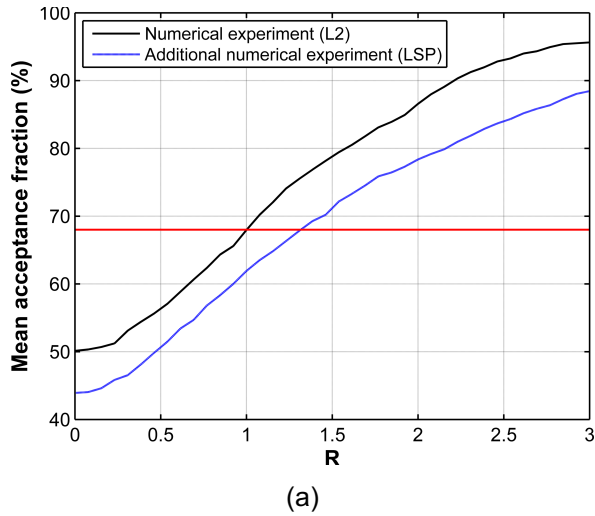
Fig. 18 – Mean acceptance fraction as a function of R for (a) numerical experiments (with 50 iterations of random noise), and for (b) repeatability experiments. Note: LSP is a different numerical experiment (not shown) and Shot peened Al and LSP SS are different repeatability experiments (not shown)
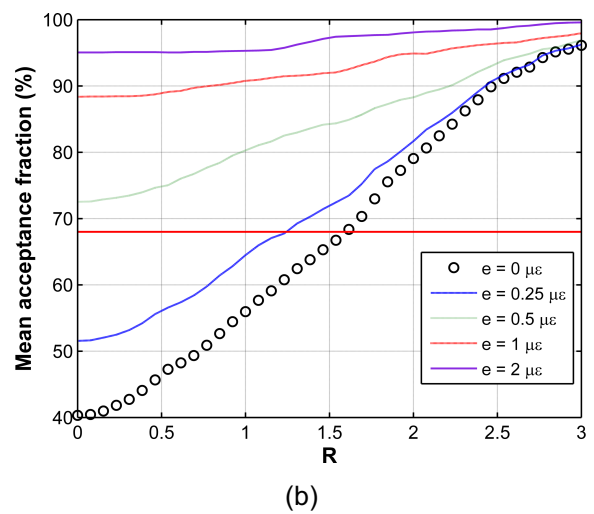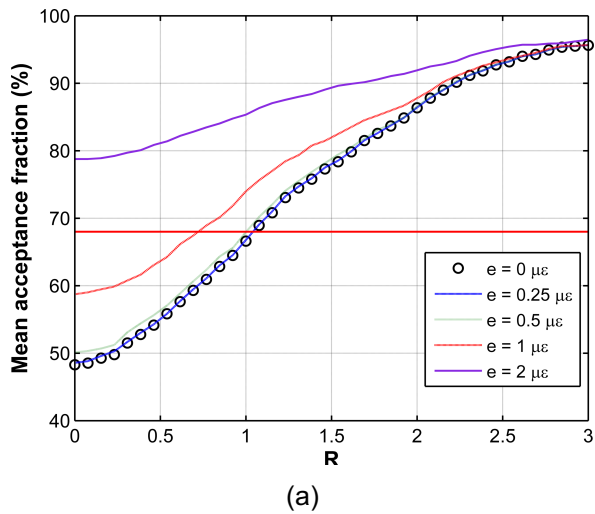

Fig. 19 – Mean acceptance fraction as a function of R for various values of e when the magnitude of the noise added to the initialized strain is (a) 1 με and (b) 0.25 με
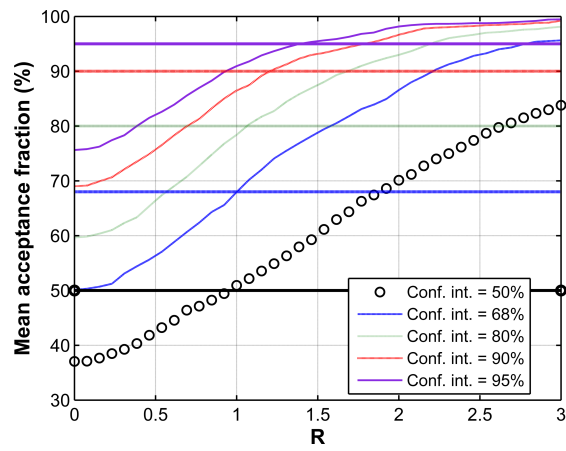
Fig. 20 – Mean acceptance fraction as a function of R for the numerical experiment for several different confidence intervals